



HAL
open science

Navier-Stokes Compatible Formulation of a Database Approach for Laminar-Turbulent Transition Prediction

Guillaume Bégou, Hugues Deniau, Olivier Vermeersch, Grégoire Casalis

► **To cite this version:**

Guillaume Bégou, Hugues Deniau, Olivier Vermeersch, Grégoire Casalis. Navier-Stokes Compatible Formulation of a Database Approach for Laminar-Turbulent Transition Prediction. *AIAA Journal*, 2017, 55 (11), page 3648-3660. 10.2514/1.J056018 . hal-01712142

HAL Id: hal-01712142

<https://hal.science/hal-01712142>

Submitted on 19 Feb 2018

HAL is a multi-disciplinary open access archive for the deposit and dissemination of scientific research documents, whether they are published or not. The documents may come from teaching and research institutions in France or abroad, or from public or private research centers.

L'archive ouverte pluridisciplinaire **HAL**, est destinée au dépôt et à la diffusion de documents scientifiques de niveau recherche, publiés ou non, émanant des établissements d'enseignement et de recherche français ou étrangers, des laboratoires publics ou privés.

Navier-Stokes Compatible Formulation of a Database Approach for Laminar-Turbulent Transition Prediction

Guillaume Bégou*, Hugues Deniau† Olivier Vermeersch‡

Onera – The French Aerospace Lab, F-31055, Toulouse, France

and Grégoire Casalis‡

University of Toulouse, ISAE, F-31055, Toulouse, France

This paper presents a transition prediction model that adds additional equations to the Reynolds-Averaged Navier Stokes set. It is based on the so-called N-factor method, valid for natural transition on wings due to the hypothesis it relies on (modal instabilities disturbing the boundary layer). It consists in an integration of the disturbances growth rates along the edge streamline. Herein, the disturbances growth rates are obtained *via* a database approach, Onera’s so-called Parabolas method. Numerically, integration of the growth rates along the edge streamline is performed through additional transport equations, thus removing the need for any topology specification from the end user. Implementation caveats are illustrated on the ONERA-D airfoil in incompressible conditions. This method is then successfully applied for transition prediction on a 2D industrial laminar airfoil at transonic conditions, with varying upstream conditions and angle of attack. Satisfactory agreements with both experimental data and conventional transition predictions (LLS stability results) are obtained which illustrates the accuracy of the predicted transition location.

*Ph.D. Candidate, Aerodynamics and Energetics Modeling Department (DMAE-ITAC)

†Ph.D. and Research engineer , Aerodynamics and Energetics Modeling Department (DMAE-ITAC)

‡Professor and research deputy-director

Nomenclature

φ^*	Dimensionless quantity corresponding to φ	ν_e	Kinematic viscosity at the boundary-layer edge
AoA	Angle of attack	N	N-factor
α	Longitudinal wave-number	N_{env}	Envelope N-factor
a, b, ε	Coefficients of diagnostic function D	N_T	Transitional N-factor value
L	Airfoil chord	$P_{i\infty}$	Upstream total pressure
C_L	Lift coefficient	ρ	Density
δ	Boundary-layer thickness	ρ_e	Density at the boundary-layer edge
δ_1	Compressible displacement thickness	Re_L	Reynolds number based on the airfoil chord
D	Diagnostic function for δ estimation	Re_{δ_1}	Reynolds number based on δ_1
f, F	Dimensional and reduced frequency	$Re_{\delta_{1tr}}$	Value of Re_{δ_1} at the transition location
	$F = 2\pi f\nu_e/u_e^2$	Re_θ	Reynolds number based on θ
f_{tr}	Frequency of the mode triggering transition	$Re_{\theta_{cr}}$	Value of Re_θ at the critical abscissa
γ	Intermittency function	$Re_{\theta_{tr}}$	Value of Re_θ at the transition location
Γ_{att}	Stagnation line indicator	σ	Growth rate of a given mode
σ_{att}	Stiffness coefficient for \tilde{I} when $\Gamma_{\text{att}} = 1$	$\sigma_{\tilde{s}}$	Growth rate for the advection of \tilde{s}
Γ_{env}	Envelope indicator (1 if $N_{\text{env}} > N_T$)	s	Curvilinear abscissa along a streamline
σ_{env}	Stiffness coefficient for \tilde{I} when $\Gamma_{\text{env}} = 1$	s_{cr}	Curvilinear abscissa at the critical location
H_i	Incompressible shape factor	\tilde{s}	Curvilinear abscissa from the critical location
\tilde{I}	Transition indicator	$\tilde{s} = s - s_{cr}$	
K_p	Pressure coefficient	$\widetilde{s_{1en}}$	Transitional region length
LLS	Local, linear stability	t	Time variable
Λ_2	Pohlhausen's pressure parameter	θ	Momentum thickness
	$\Lambda_2 = \theta^2/\nu (du_e/dx)$	T_u	Free-stream turbulence level
M_e	Mach number at the boundary-layer edge	$T_{i\infty}$	Upstream total temperature
M_∞	Upstream Mach number	u	Boundary-layer streamwise velocity
ν	Kinematic viscosity		

u_e	Velocity at the boundary-layer edge	x_{cr}	Chord-wise critical abscissa
\vec{V}	Flow velocity vector	x_{tr}	Chord-wise transition location
ω	Angular frequency	y	Wall-normal direction
	$\omega = 2\pi f$	y_{max}	Wall distance at which D is maximum
x	Longitudinal direction		

I. Introduction

Laminar-turbulent transition prediction is of major practical interest in a range of aeronautical applications such as designing fuel-efficient laminar wings with low friction drag or assessing the effects of wall heating on boundary-layer stability in de-icing conditions.

Prediction of the transition location has thus become a challenge in modern numerical fluid dynamics and an extensive use of the so-called N-factor method has been made for the last five decades.¹ In the case of natural transition, the laminar boundary layer is contaminated by external perturbations, which are turned into normal modes through a process known as receptivity. The linear amplification of these modes is followed by non-linear interactions that trigger breakdown to transition.²

The N-factor method consists in an integration of the spatial growth rates of each mode along the edge streamline (the local projections of the loci, where the streamlines cross the boundary-layer edge). Growth rates are given by the local linear stability theory and transition is assumed to take place where the most amplified mode's N-factor — highest N-factor at a given location — reaches a prescribed transitional value.^{3,4}

As it is based on a local linear theory, this method does not account for some phenomena, such as non-parallel effects, receptivity process, and nonlinear mechanisms. The growth rate values under these assumptions may be obtained accurately *via* a local linear stability study that can be very time-consuming (when compared with the computation time of a single RANS iteration).

Over the last two decades, Onera has developed a simplified growth rates computation method that requires a much lower computational effort. It is based on a simple closed-form approximation of the growth rates, function of the Reynolds number and a dimensionless frequency. The different coefficients used in the closed-form expressions are tabulated with respect to some relevant flow parameters (integral thicknesses for instance). This method is referred to as a database approach or Parabolas method and was firstly

developed for two-dimensional compressible flows over adiabatic walls.⁵ It was then extended to compressible three-dimensional flows⁶ with a correction for wall temperature effects. This extension addresses separately crossflow and Tollmien-Schlichting instabilities. The complete method was implemented in the boundary-layer solver 3C3D as this type of solver enables easy access to the aforementioned relevant flow parameters and has been successfully applied to complex configurations.

To obtain the N-factors, the growth rates computed with this method then have to be numerically integrated over the edge streamline. In a RANS code, the determination of the edge streamline can be challenging as it requires an accurate determination of the boundary-layer thickness. Once the edge streamline has been defined, carrying out the integration involves numerous interpolations from the mesh to the line, which complicates the matter.

A method where the integration over a streamline is recast into an advection equation with a source term is proposed in this paper. The resulting new set of transitional equations is then solved similarly to the mean flow and turbulence equations.

This paper is divided in four parts followed by conclusions. Section II details the N-factor method and gives a state of the art of its application in RANS solvers. Section III introduces the Parabolus method and the set of equations implemented in the RANS solver. Validations and tests are covered in sections IV and V. The former consists in an ONERA-D airfoil used as a tutorial case while the latter gives results obtained on a transonic laminar airfoil and compared against experimental data and LLS stability results.

II. State of the art: N-factor method

The developments presented in this paper are restricted to two-dimensional mean flows, without crossflow instabilities. As a consequence, only Tollmien-Schlichting waves will be taken into account. Furthermore, only two-dimensional instabilities will be considered. This is justified for the incompressible test cases by Squire's theorem⁷ and for the compressible test cases by local linear stability studies that showed that the most amplified perturbations are indeed two dimensional.

II.A. Instability amplification

II.A.1. Local linear stability theory

As stated in the introduction, natural transition occurs when the boundary layer is disturbed by a set of perturbations (noise, external turbulence...) transformed through a process called receptivity into a set of small perturbations that grow or decay in the form of normal modes.⁸ A local spatial stability analysis allows the determination of unstable modes. Velocity, pressure and temperature are written as

$$\varphi^* = \bar{\varphi} + \varphi' , \quad (1)$$

where φ^* is the dimensionless quantity, $\bar{\varphi}$ its mean value and φ' its fluctuation which modal form yields

$$\varphi' = \underbrace{\varphi' (y^*)}_{\text{eigen-}} \underbrace{e^{\sigma^* x^*}}_{\text{growth-}} \underbrace{e^{i(\alpha^* x^* - \omega^* t^*)}}_{\text{shapefunction}} + \text{C.C.} \quad (\text{C.C.} = \text{complex conjugate}). \quad (2)$$

Where σ^* is the dimensionless growth rate, α^* the dimensionless longitudinal wave-number, and ω^* the dimensionless angular frequency. They are defined with respect to their dimensional (unstarred) counterparts by

$$\sigma^* = \sigma \delta_1 , \quad \alpha^* = \alpha \delta_1 \quad , \quad \text{and} \quad \omega^* = \omega \frac{\delta_1}{u_e} = 2\pi f \frac{\delta_1}{u_e} , \quad (3)$$

where δ_1 is the compressible displacement thickness and f is the mode's dimensional frequency. All these quantities are real-valued in the context of spatial stability .

A mode is amplified when its growth rate σ is positive and damped otherwise. The quantity F is a characteristic reduced frequency used to perform stability analysis and is defined as

$$F = \frac{2\pi f \nu_e}{u_e^2} = \frac{\omega}{\text{Re}_{\delta_1}} \frac{\delta_1}{u_e} = \frac{\omega^*}{\text{Re}_{\delta_1}} , \quad (4)$$

where Re_{δ_1} is the Reynolds number based on the compressible displacement thickness δ_1 .

Stability analysis can be made by injecting the form of instabilities proposed in relation (2) into the linearized Navier-Stokes equations. This leads to the Orr-Sommerfeld equation in the incompressible case

and more generally to a local, linear stability (LLS) problem, which can be numerically solved — for a given mean flow — to obtain the growth rates of several frequencies as functions of both $\text{Re}\delta_1$ and ω^* .

The frequency band where instabilities are amplified can be visualized on a so-called stability diagram, an example of which is shown in figure 1(a). In this ω^* - $\text{Re}\delta_1$ diagram, iso-frequencies (iso- F) are straight lines passing through the origin ($\omega^* = F \text{Re}\delta_1$) and iso growth-rates (iso- σ^*) are represented. The neutral curve is defined as the set of points for which $\sigma^* = 0$ and delimits the stable and unstable regions. The critical point is the location of the neutral curve with the lowest $\text{Re}\delta_1$.

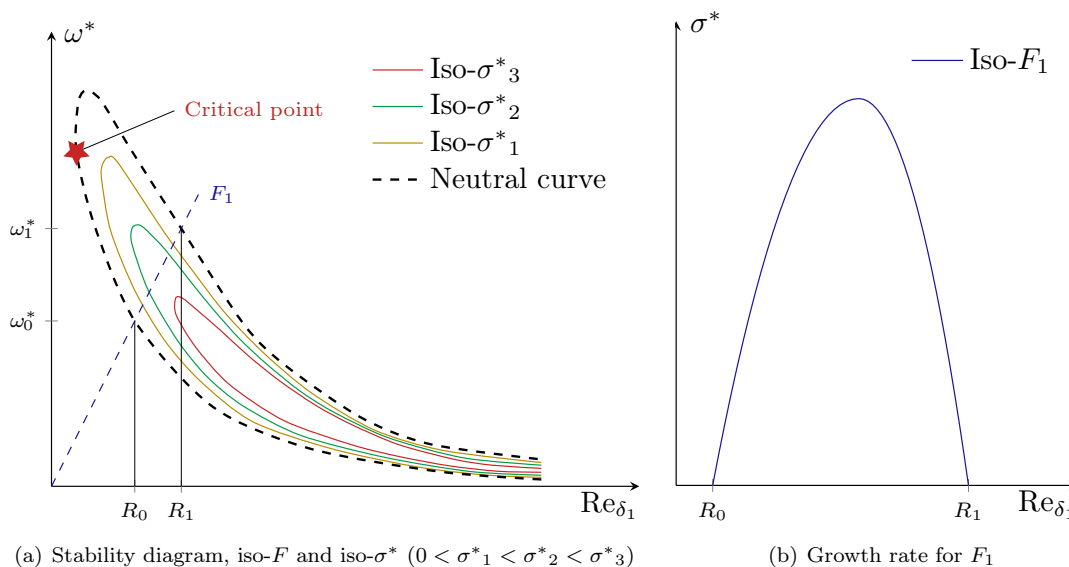


Figure 1. Example of stability diagram and growth-rate diagram.

Arnal⁵ observed that the growth rate — presented figure 1(b) — of a given F as a function of $\text{Re}\delta_1$ can be approximated by two half parabolas as explained in section III.

II.A.2. N -factor method

The N -factor method is a technique where the total amplification N of each unstable mode is computed. Let us consider a given mode of initial amplitude A_0 at a location x_{cr}^* , that increases up to an amplitude A at a location x^* . This mode's exponential growth yields the expression of N integrated along the boundary-layer edge streamline

$$N(s, f) = \ln \frac{A}{A_0} = \int_{s_{cr}}^s \sigma(F(f, \eta), \eta) d\eta. \quad (5)$$

where s is the curvilinear abscissa along the edge streamline

$$s = s(x^*) \quad s_{cr} = s(x_{cr}^*) .$$

A semi-empirical correlation established by Mack⁹ provides an estimation of the transitional N-factor N_T for Tollmien-Schlichting modes as a function of the upstream turbulence level T_u

$$N_T = -8.43 - 2.4 \ln(T_u) \quad 10^{-3} < T_u < 10^{-2} \quad (\implies N_T \in]2.6 ; 8.2[) . \quad (6)$$

The N-factor of several modes are computed and the curve given by $N_{env} = \max_f(N)$ — called the envelope — is obtained. Transition is attained at a location noted x_{tr}^* where the envelope crosses the transitional N-factor N_T , as represented figure 2.

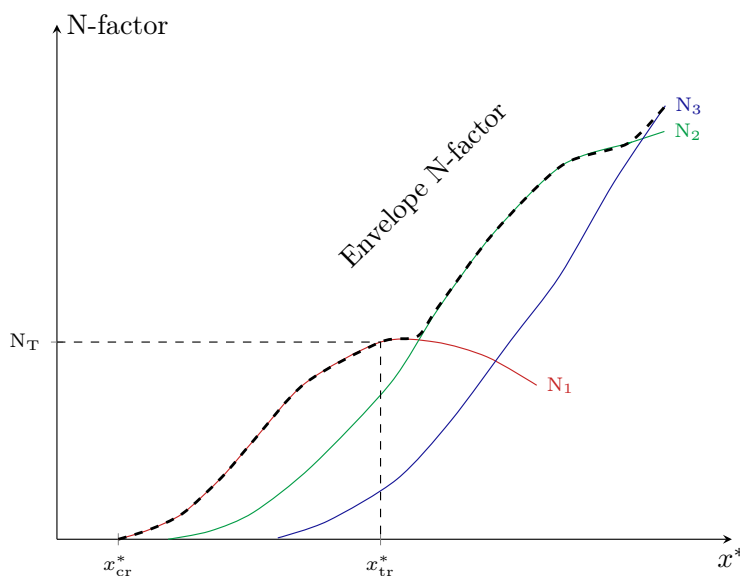


Figure 2. Envelope technique for the N-factor method with three frequencies.

The physical growth rate σ of each of these modes has to be known at each streamwise station to compute the value of N . To do so, one can either use exact stability results (*via* the LLS equation for instance) or, as it is done here, use a simplified method such as the so-called database method developed at Onera.

II.B. Transition prediction in a RANS solver

Simplified methods are needed to compute the transition location in a RANS solver because of the numerical cost of solving the LLS equation during a RANS iteration as mentioned in the introduction. It also avoids the resolution of the LLS problem based on RANS velocity profiles that may lack accuracy. They consist in a simplified formulation of either the N-factor or the growth rates.

II.B.1. N-factor computation simplification: transition criteria

The first category results in a variety of transition criteria, such as those established by Gleyzes,¹⁰ Abughannam and Shaw¹¹ (ABS) and Arnal, Habiballah, and Delcourt¹² (AHD).

The Gleyzes criterion gives the slope of the envelope N-factor as a function of the Reynolds number based on the momentum thickness for separated flows. Drela¹³ expressed a similar N-factor-slope law $\partial N_{\text{env}}/\partial \text{Re}_\theta$ valid for both attached and separated flows and an empirical relation to get $\partial \text{Re}_\theta/\partial x$. He applied the resulting ODE

$$\theta \frac{dN_{\text{env}}}{dx} = f_{\text{Drela}}(H_i, \text{Re}_\theta) \quad (7)$$

in the MISES solver. This implementation was then extended with the ABS transition criterion for bypass transition. It compares Re_θ to its critical value $\text{Re}_{\theta_{cr}}$ where instabilities begin to grow, given by a correlation based on T_u and Polhausen's pressure parameter Λ_2 . Drela¹⁴ recast the ABS criterion into a N-factor-slope law and obtained a form similar to the ODE he obtained for the Tollmien-Schlichting modes yielding his final envelope ODE

$$\theta \frac{dN_{\text{env}}}{dx} = f_{\text{Drela,TS}}(H_i, \text{Re}_\theta) + f_{\text{Drela,ABS}}(H_i, \text{Re}_\theta) . \quad (8)$$

The main shortcoming of this approach is that the N_{env} slope expression is based on a constant H_i hypothesis.

To overcome this, Drela¹⁵ expressed the non-dimensionalized Orr-Sommerfeld equation as a database by considering the velocity profiles as self-similar profiles indexed by H_i . The resulting database indexes the growth rate by H_i , Re_θ and $\omega\theta/u_e$, allowing the determination of the most amplified frequency at each station and the integration of the actual envelope.

Menter, Langtry *et al.*^{16,17} used a correlation to express a transition criterion into a scalar transport

equation in their well-known $\gamma - \overline{\text{Re}_\theta}$ transition model for turbomachinery applications. This correlation — valid for Blasius flows — yields the momentum thickness Reynolds number from the maximum value of the vorticity Reynolds number inside the boundary layer.

They mentioned that their model does not attempt to represent the physics of the transition process and its first version (referred to as CFX-v1.0) was rather devised to behave like several criteria. At high turbulence levels ($T_u > 3\%$), it is based on the Mayle correlation.¹⁸ At moderate turbulence levels ($1\% < T_u < 3\%$) and pressure gradients it is similar to the ABS criterion. Finally, it has been curve fit to agree with Drela's¹⁴ second model in low turbulence levels ($T_u < 1\%$). It was later extended by Langtry¹⁹ (CFX-v1.1) who changed the correlation for the integral boundary-layer quantities from its Blasius value to $H_i = 3.5$ and modified the whole model coefficients to improve its prediction capabilities in the case of natural transition.

Drela's first approach¹³ to express the Tollmien-Schlichting modes was later recast by Coder²⁰ into a transport equation in a RANS solver. The main part of the reformulation was to turn the model into a local model since it relies on integral quantities. This was done by defining a pressure gradient parameter H_L computed from the magnitude of the strain-rate tensor, the distance to the nearest wall and u_e — obtained from the local pressure with an isentropic flow condition. The shape factor H_i is then obtained through a correlation based on H_L calibrated with a set of Falkner-Skan-Hartree profiles to take pressure gradient effects into account.

The AHD criterion is also an approximation of the envelope N-factor for the TS modes as

$$N_{\text{env}}(\text{Re}_\theta - \text{Re}_{\theta_{\text{cr}}}, \Lambda_2) , \quad (9)$$

giving at the transition location

$$N_{\text{env}}(\text{Re}_{\theta_{\text{tr}}} - \text{Re}_{\theta_{\text{cr}}}, \Lambda_2) = N_{\text{T}} . \quad (10)$$

This criterion expresses²¹ $\text{Re}_{\theta_{\text{tr}}} - \text{Re}_{\theta_{\text{cr}}}$ as a function of Λ_2 and T_u , and $\text{Re}_{\theta_{\text{cr}}}$ as a function of H_i . This formulation of the criterion is only valid for self-similar flows and has been extended to general flow configurations by averaging Λ_2 along the edge streamline. It was implemented in the RANS solver *elsA*²² which was applied for the work presented in this article (see section IV) along with the Gleyzes criterion by Cliquet *et al.*²³ In their case, integration is carried out along wall mesh-lines aligned with the flow direction. The

mesh lines to use to perform the integration are selected in a user-given topology file, which complicates the data entry step. The major drawback of this approach is that the mesh lines are considered to be aligned with the edge streamline. The curvature of the edge streamline is thus not taken into account in the case of three-dimensional flows.

II.B.2. Growth rate computation

As mentioned earlier another approach is to compute the growth rates *via* a simplified method: a look-up table or a neural network for instance. This type of approach yields higher levels of accuracy. Different types of database exist: van Ingen¹ made one with complete stability diagrams while Drela¹⁵ or Stock²⁴ store the growth rate values. The Parabolus method presented in the next section is another type of database approach.

Neural networks have been developed by Fuller *et al.*²⁵ and Crouch *et al.*²⁶ for instance. The former was designed for shear layers and its inputs are the angular frequency, the azimuthal mode number and the shear-layer momentum thickness while the latter is designed as a replacement of the LLS equation expressed with integral quantities. Its inputs are the Reynolds numbers based on the longitudinal and transverse displacement thickness, the reduced frequency, the edge streamline direction and a set of values of the first derivative of the longitudinal and transverse velocity profiles.

The input data of both databases or neural networks are either velocity profiles or integral thicknesses.

The computation and integration of the growth rates can be embedded in an external transition module. It is then possible to couple this transition module with the RANS solver. For instance, Krumbein²⁷ used this type of coupling where the RANS solver FLOWer²⁸ gives the surface pressure distribution that is processed through a boundary-layer solver to get the velocity profiles used as an input to Stock's database to eventually compute the transition location. Gross *et al.*²⁹ also applied this type of approach in the industrial Dassault Aviation solver Aether (a finite element RANS solver, a description of which is given in Chalot *et al.*³⁰). In this case, the boundary-layer velocity profiles and the transition were computed *via* Onera's boundary-layer solver 3C3D, either with the Parabolus method or transition criteria. 3C3D is a three-dimensional boundary layer code based on a characteristic method,³¹ resolving the boundary layer equations on a wall normal mesh and has been extended with a number of transition prediction tools.⁶

The boundary-layer solvers need either the values of the boundary-layer external velocity (which requires a well-refined mesh in the boundary layer region along with an external velocity extraction method) or a wall pressure distribution (associated to a 2D, conical or infinite swept wing hypothesis to compute the boundary-layer edge velocity).

The method proposed in this paper computes the growth rates *via* the Parabolus method and reformulates the N-factor integration into a transport equation. The Parabolus method requires boundary-layer quantities that are directly obtained within the RANS solver. Two complex issues of the aforementioned methods are therefore circumvented:

- Computing the boundary-layer quantities and growth rates within the RANS solver avoids the use of any coupling with an external solver.
- The transport equation formulation avoids explicitly integrating the growth rates and intrinsically follows the edge streamline.

III. Current implementation of the N-factor method in a RANS code

III.A. Database approach and RANS boundary-layer quantities

At low speed the occurrence of instabilities is mainly due to viscous phenomena as established by Prandtl.³² The dimensionless growth rates are expressed in the closed-form (11) with two half parabolus as presented in figure 3, yielding

$$\frac{\sigma^*}{\sigma_M} = 1 - \left[\frac{\text{Re}_{\delta_1} - R_M}{R_k - R_M} \right]^2, \quad (11a)$$

where

$$R_k = \begin{cases} R_0 & \text{Re}_{\delta_1} < R_M \\ R_1 & \text{Re}_{\delta_1} > R_M \end{cases}. \quad (11b)$$

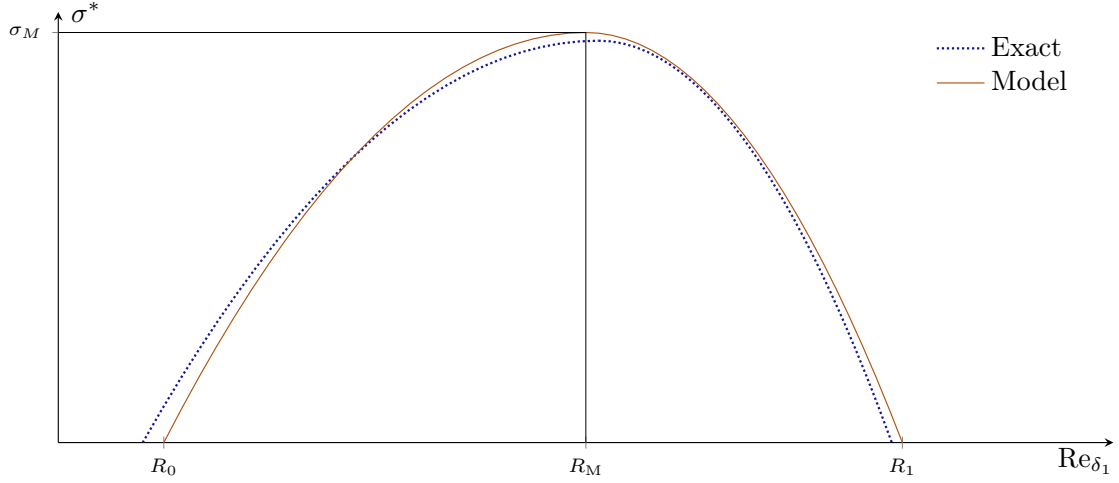


Figure 3. Qualitative comparison of exact and approximate viscous growth rates (iso- F).

The parabolas parameters σ_M , R_M , R_0 and R_1 are functions of the reduced frequency F as follows

$$\sigma_M = A_M \left(1 - \frac{F}{F_M} \right), \quad (12)$$

$$R_M = K_M (10^5 F)^{E_M}, \quad (13)$$

$$R_0 = R_M \left[1 - A_0 \left(1 - \frac{F}{F_0} \right) \right], \quad (14)$$

$$R_1 = R_M \left[1 - A_1 \left(1 - \frac{F}{F_1} \right) \right]. \quad (15)$$

The 8 coefficients A_M , F_M , K_M , E_M , A_0 , F_0 , A_1 , and F_1 are stored in a database indexed on the incompressible shape factor H_i and the external Mach number M_e . They have been determined⁵ from the exact stability diagram of numerous Falkner-Skan-Hartree³³ similarity profiles. Negative growth rates (disturbance decaying) are obtained by a simple linear extension of the parabolas.

At higher velocities instabilities may come from the presence of an inflection point in the velocity profiles,³⁴ taken into account through an additional dedicated set of two half-parabolas.⁶ A description of the complete Parabolas method for TS waves is given in the appendix.

It is therefore necessary to be able to determine these quantities within the RANS solver and particularly the boundary-layer thickness. To do so the RANS solver used, *e/sA*, embeds the concept of lines normal to the wall. They are called pseudo-normals and are defined by following a mesh line starting at the wall and ending at the boundaries of the computational domain, going through mesh block joins.

It is therefore possible to associate to each field cell in the computational domain a wall cell defined as the root of the pseudo-normal line passing through this field cell.

At each iteration and along each pseudo-normal line it is then possible to determine the boundary-layer thickness. A procedure proposed by Stock and Haase³⁵ is used to do so. It is based on a diagnostic function D , evaluated along each pseudo-normal and defined as

$$D = y^a |\Omega|^b , \quad (16)$$

where y is the wall normal distance along the pseudo-normal line and $|\Omega|$ is the vorticity vector modulus. The wall distance y_{\max} is then defined as

$$D|_{y_{\max}} = \max(D) , \quad (17)$$

and leads to the boundary-layer thickness through

$$\delta = \varepsilon y_{\max} . \quad (18)$$

Two sets of the three coefficients a , b and ε were determined by Stock and Haase for laminar and turbulent reference mean profiles.

A boundary-layer velocity profile is considered along each pseudo-normal line. The boundary-layer integral quantities are then computed by integrating the velocity profile *via* a trapezoidal rule and the boundary-layer edge quantities such as M_e are extracted at δ . It is then possible to compute for each pseudo-normal line the corresponding σ^* *via* the Parabolus method.

In the end, each field cell has associated values of σ^* , boundary-layer integral and edge quantities, and a corresponding wall cell. Every field cell on the same pseudo-normal line therefore has the same values of σ^* and boundary-layer quantities as well as the same corresponding wall cell. These values are stored at the wall cells.

III.B. N-factor method reformulation into a set of transport equations

Herein, unless explicitly mentioned, the functions are evaluated at (\vec{x}, t) and s is the curvilinear abscissa along a pathline. We will consider a generic definition of the N-factor along any pathline as

$$N(s, f) = \ln \frac{A}{A_0} = \int_{s_{cr}}^s \sigma(F(f, \eta), \eta) \, d\eta, \quad (19)$$

that can be differentiated to determine the N variation seen by a flow particle moving from \vec{x} to $\vec{x} + \Delta t \vec{V}$ between t and $t + \Delta t$. This yields on one hand

$$N(\vec{x} + \Delta t \vec{V}, t + \Delta t) = N + \sigma \|\vec{V}\| \Delta t + \mathcal{O}(\Delta t^2), \quad (20)$$

while a first order Taylor approximation gives on the other hand

$$N(\vec{x} + \Delta t \vec{V}, t + \Delta t) = N + \Delta t \vec{V} \cdot \overrightarrow{\text{grad}} N + \Delta t \frac{\partial N}{\partial t} + \mathcal{O}(\Delta t^2). \quad (21)$$

These two expressions can be combined into

$$\frac{\partial N}{\partial t} + \overrightarrow{\text{grad}} N \cdot \vec{V} = \frac{DN}{Dt} = \sigma \|\vec{V}\|. \quad (22)$$

The mass conservation equation ($\partial \rho / \partial t + \text{div}(\rho \vec{V}) = 0$) finally yields the conservative form

$$\frac{\partial \rho N}{\partial t} + \text{div}(\rho N \vec{V}) = \rho \|\vec{V}\| \sigma. \quad (23)$$

The ‘‘classical’’ integral (19) carried along the edge streamline has thus been generalized into an advection equation (23) on the whole computational domain with a source term $\rho \|\vec{V}\| \sigma$. This type of equation is better suited to a RANS solver than the original integral formulation since it avoids (see section IV):

- Finding the integration path (the edge streamline geometry).
- Performing the integration along this path (thus requiring interpolations from the initial mesh to the integration path).

To ensure that the N-factors are integrated starting from a null value, an additional forcing term is added to the source term. It sets the N-factor value to 0 in field cells whose corresponding wall cells are near the stagnation point (see figure 4). The resulting complete equation is as follows

$$\frac{\partial \rho N}{\partial t} + \text{div}(\rho N \vec{V}) = \rho \|\vec{V}\| \sigma - \Gamma_{\text{att}} \sigma_{\text{att}} \rho N, \quad (24)$$

where σ_{att} is a forcing stiffness coefficient set to 1.1 and

$$\Gamma_{\text{att}} = \begin{cases} 1 & \text{if wall cell is in stagnation region} \\ 0 & \text{otherwise} \end{cases}. \quad (25)$$

The determination of the stagnation regions is done *via* the method proposed by Kenwright *et al.*³⁶ at each iteration in the RANS solver. The forcing term has no effect when $\Gamma_{\text{att}} = 0$ and a zero wall-normal flux condition is applied at the other wall cells.

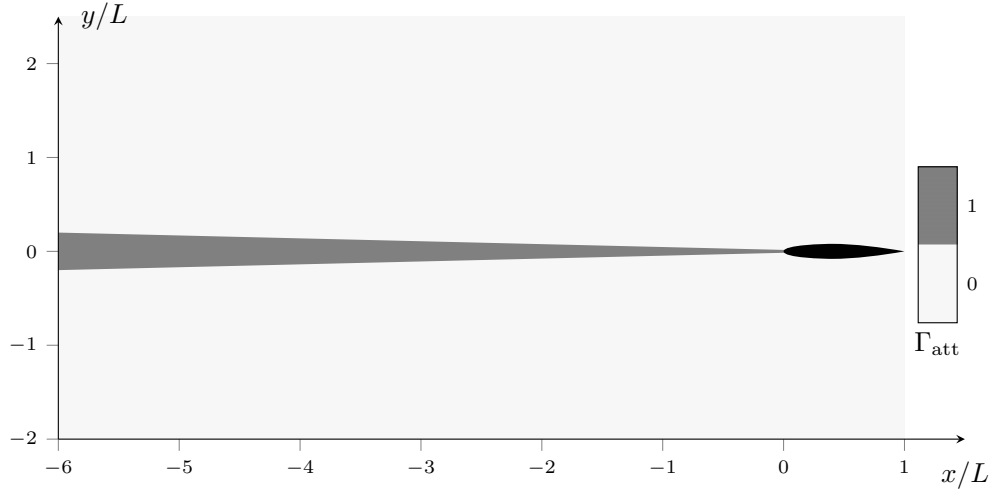


Figure 4. Stagnation line indicator.

The N-factor value needed to determine whether transition occurs is then extracted at the boundary-layer edge. The solving method is as follows, for every iterations of a RANS computation:

1. Compute the growth rates σ^* of each N-factor — each physical frequency f — *via* the database approach. The method used in this paper to prescribe the frequency range is given in section IV.A .

2. Compute the local source term $\rho \left\| \vec{V} \right\| \sigma = \rho \left\| \vec{V} \right\| \sigma^* / \delta_1$ on the whole computational domain. It is reminded that σ^* and δ_1 come from the computations made along the corresponding pseudo-normal line (see section III.A).
3. Solve an advection equation for each ρN , decoupled from the mean state equations (the values of \vec{V} for the determination of N at iteration $n + 1$ are taken from iteration n).
4. Extract the N -factor value ($\rho N / \rho$) at the boundary-layer edge.
5. For each station on the wing, compare the value of the maximum extracted N -factor (N_{env}) to N_T .
6. If the maximum is higher than N_T , the turbulence model is activated.

This method's major drawback is its memory cost: solving an equation on the complete domain for each N -factor implies that values of ρN have to be stored in each mesh cell and for each N -factor although we only need the values on a single line (the boundary-layer edge). Then again, this specific single line is not known and difficult to determine in a RANS computation.

It also requires the computation of the boundary-layer thickness and integral quantities, which is possible in *elsA*. This turns the N -factors transport equations into a non-local model since the values of σ^* and δ_1 for a given field cell correspond to the pseudo-normal line passing through this field cell. The values of N_{env} are also stored in the wall cells.

IV. First validations: transition prediction on the ONERA-D airfoil

The RANS solver used is *elsA* (version 3.4). It is based on an object-oriented programming language. It solves the Navier-Stokes equations on structured meshes with a cell-centered finite volume discretization technique. A backward Euler time integration scheme is used with a local time step. Implication is performed *via* a scalar lower-upper successive over-relaxation (LU-SSOR) method.

The transition is taken into account through the effective viscosity concept (Boussinesq eddy viscosity assumption) $\mu_{\text{eff}} = \mu + \gamma \mu_t$ where γ is the intermittency factor ($\gamma = 0$ if the flow is laminar, $\gamma = 1$ if it is turbulent) and μ_t is given by the turbulence model used. The intermittency factor γ is stored in the wall cells and applied to all field cells on the corresponding pseudo-normal (see III.A). It can either be a user-defined

value to force the transition location or be set by a transition model.

The ONERA-D airfoil is a symmetrical supercritical airfoil and the conditions set for the tests are subsonic incompressible ($M_\infty = 0.17$). The mesh used is well refined in the boundary layer (about 50 mesh points within the boundary layer in the wall-normal direction). The turbulence is computed *via* Menter's $k-\omega$ SST model³⁷ and Roe's numerical scheme³⁸ is used with a third order MUSCL flux reconstruction and no limiter.

A two-step approach is used:

1. A first solution is obtained with a fixed arbitrary transition location (user-defined intermittency factor distribution at the wall) as close to the trailing edge as possible (but close enough to the leading edge to avoid any laminar separation that might prevent convergence).
2. This first solution is used as an initial state for the actual computation, where the Parabolus method is used to determine the transition location.

This two-step approach is needed on one hand to avoid applying the Parabolus method to erratic values of boundary-layer quantities and on the other hand because the method yields the growth rates of perturbations disturbing a laminar boundary layer.

The purpose of this test case is to identify and tackle numerical issues. This section is broken down into three parts. Section IV.A assesses the validity of the transport equations as a replacement of the integral formulation and section IV.B explains the need for a transition indicator while convergence issues are addressed in section IV.C.

IV.A. Transport equation validation

The first step is to verify whether the proposed transport equation (24) is actually equivalent to the original integral formulation (19). To do so, a standalone in-house code is used (referred to as FENEC) designed specifically for validation purposes. Its inputs are the boundary-layer quantities computed with *elsA* and it computes the growth rates of the desired frequencies *via* the Parabolus method. The integration of the N-factors (19) in FENEC is carried out along the airfoil's curvilinear abscissa. FENEC is also used to find out a range of unstable frequencies, using the boundary-layer quantities given by *elsA* at step 1. *elsA*'s transport equation results are then compared against FENEC to assess their accuracy. The N-factor values

in this case are not used for the onset of transition (transition is arbitrarily fixed at $x/L = 60\%$). Results are plotted in figure 5.

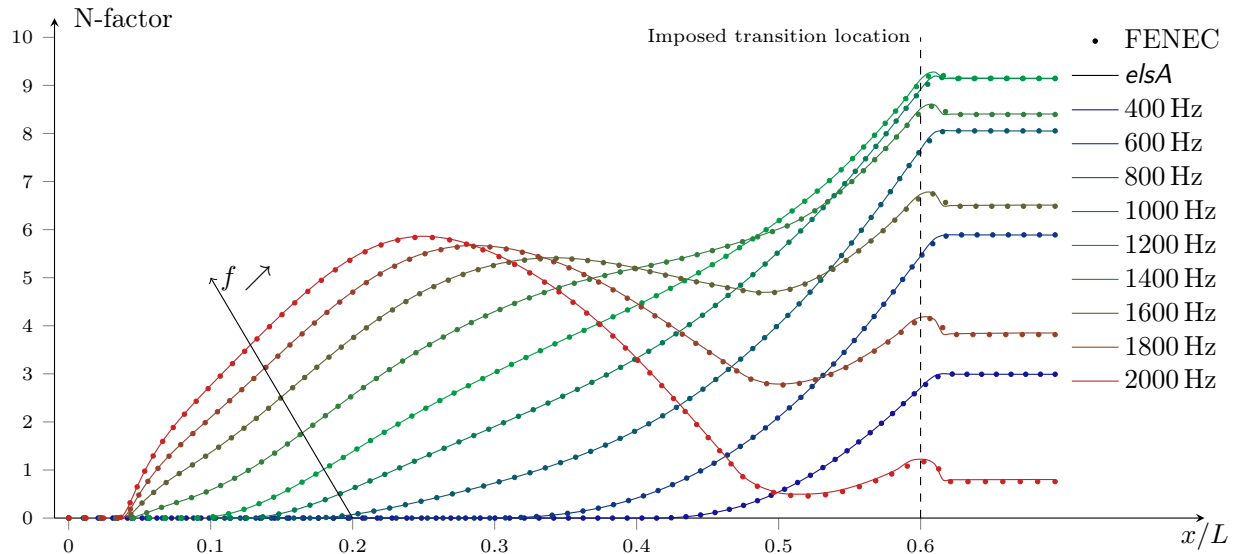


Figure 5. Comparison between exact integration results (symbols) and transported N-factor (lines).

The N-factors values computed by FENEC and *elsA* are in excellent agreement, which confirms that both the N-factors computation *via* a transport equation and their extraction at the boundary-layer edge are valid in *elsA*. To avoid computing the damping of modes that have not yet been amplified the following condition is applied:

$$\sigma := \max(0, \sigma) \quad \text{when} \quad N < 0.5 .$$

While this condition works well to avoid damping modes that have not yet been amplified, its side effect is to prevent the N-factor from dropping below the arbitrary value of 0.5. This limiter should not have any impact on the transition prediction as it can be considered that a N-factor damped down to 0.5 is unlikely to be re-amplified enough to contribute to the envelope.

IV.B. Transition indicator

A problem arises when trying to use the N-factors to trigger transition instead of using an imposed transition location: to know if a field cell is downstream of the transition location, it is necessary to know if the N-factor envelope already reached a value higher than N_T somewhere upstream on the corresponding pathline. It is indeed not sufficient to check the value of N_{env} (stored in the corresponding wall cell) against N_T since

no assumption can be made on the envelope evolution. N_{env} could increase up to N_T , triggering transition, but then decrease below this threshold in the turbulent region. In such a situation, the decrease does not correspond to relaminarization and should not be taken into account.

To the best of the authors' knowledge, the only way to get access to an information available upstream of the current location is to transport the said information. As a consequence, a transition indicator \tilde{I} is advected. It follows a classical convection equation with a source term used to apply two types of forcing. The first one sets the indicator value at 0 in field cells whose associated wall cells are near the stagnation point (as it was done for the N-factor transport equation (24)). The second one sets it at 1 when the envelope is greater than N_T . The resulting transport equation is

$$\frac{\partial \rho \tilde{I}}{\partial t} + \text{div} \left(\rho \tilde{I} \vec{V} \right) = -\Gamma_{\text{att}} \sigma_{\text{att}} \rho \tilde{I} - \Gamma_{\text{env}} \sigma_{\text{env}} \rho \left(\tilde{I} - 1 \right) , \quad (26)$$

where σ_{att} and σ_{env} are forcing stiffness coefficients set to 1.1 and

$$\Gamma_{\text{att}} = \begin{cases} 1 & \text{if wall cell is in stagnation region} \\ 0 & \text{otherwise} \end{cases} \quad \text{and} \quad \Gamma_{\text{env}} = \begin{cases} 0 & N_{\text{env}} < N_T \\ 1 & N_{\text{env}} \geq N_T \end{cases} . \quad (27)$$

The two forcing terms are not supposed to be activated at the same time. Figure 6(a) shows a synthetic situation where the value of $N_T = 5.5$ has been chosen to represent the pathological case where a “relaminarization” could be detected. In that case, the transition indicator is forced at 1 where $N_{\text{env}} > N_T$, at 0 in the stagnation region and advected elsewhere. After a transient phase (figures 6(b) and 6(c)) the converged indicator has the desired values (figure 6(d)): 0 before the envelope reaches N_T and 1 after, even at the locations where $N_{\text{env}} < N_T$ ($x/L \in [0.33; 0.44]$).

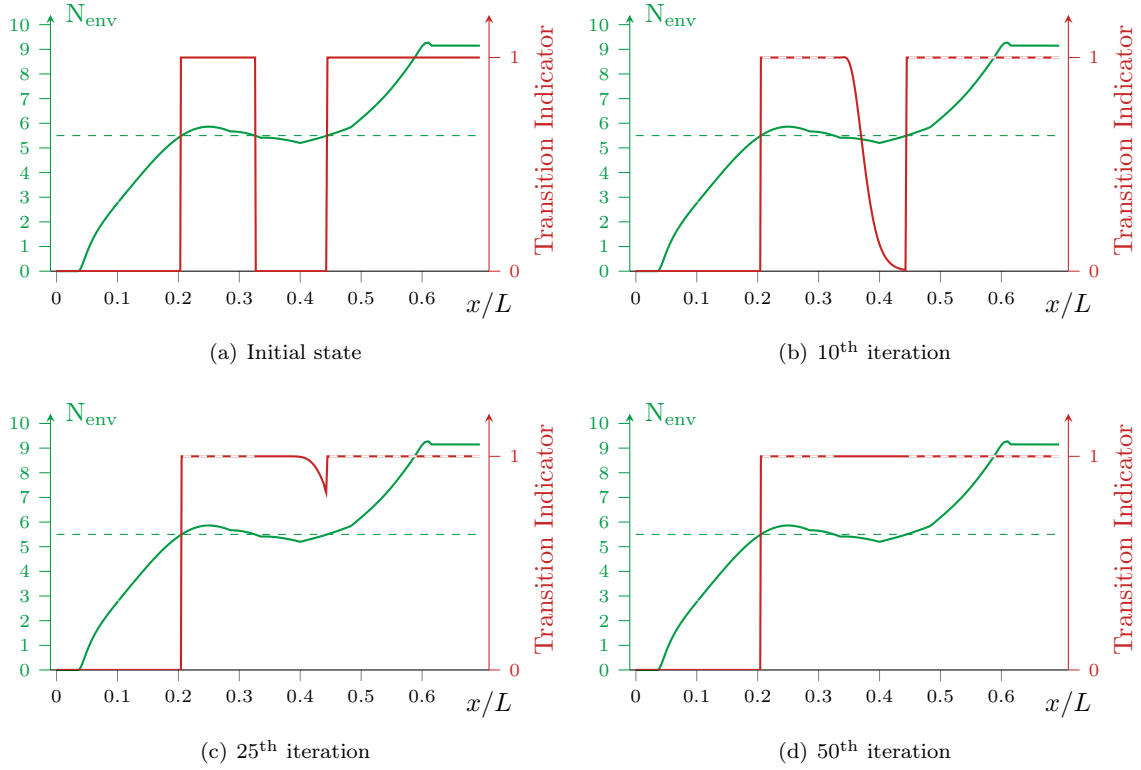


Figure 6. Transition indicator evolution (solid line: advected values, dashed line: forced values).

IV.C. Convergence issues and intermittency function

In the first implementation of the model, point transition was applied, namely

$$\gamma = \begin{cases} 0 & \tilde{I} < 0.2 \\ 1 & \tilde{I} \geq 0.2 \end{cases} . \quad (28)$$

where the arbitrary threshold 0.2 is only necessary on transient iterations since \tilde{I} might not be exactly 0 or 1 but somewhere in between.

Besides the lack of physical relevance of this type of intermittency factor distribution (it does not take the transitional zone into account where laminar regions and turbulent spots co-exist), Drela,¹⁴ and Stock and Haase³⁹ mentioned that it generates a strong viscous/inviscid interaction region that prevents the method from converging. This comes from the rapid decrease of δ_1 from its laminar value at the transition location. This viscous phenomenon acts like a sink for the inviscid flow and therefore increases its velocity upstream of the transition location. This causes the transition to be delayed, allowing δ_1 to re-increase and the transition

to be advanced back upstream and repeat the cycle. The same type of issue has been encountered in our computations and convergence could not be reached.

This establishes the need for a longitudinal intermittency function to smooth the transition from the laminar to the turbulent state of the flow. In the same study, Stock and Haase used the classical Dhawan and Narasimha⁴⁰ universal intermittency formulation to obtain

$$\gamma = 1 - \exp \left(-0.411 \left(3.36 \frac{\tilde{s}}{\widetilde{s}_{\text{len}}} \right)^2 \right) . \quad (29)$$

Where $\widetilde{s}_{\text{len}}$ is the length of the transitional region and \tilde{s} is the curvilinear abscissa starting at the transition location. $\widetilde{s}_{\text{len}}$ is unknown and needs to be modeled. Narasimha,⁴¹ Chen and Tyson,⁴² and Walker⁴³ proposed formulations of the form

$$\text{Re}_{\widetilde{s}_{\text{len}}} = A (\text{Re}_{s_{\text{tr}}})^b , \quad (30)$$

when neglecting compressibility effects. They are all based on the knowledge of $\text{Re}_{s_{\text{tr}}}$, the Reynolds number based on the curvilinear abscissa taken at the beginning of the transitional region. Stock and Haase proposed to use a correlation to deduce $\text{Re}_{s_{\text{tr}}}$ from the value of Re_{δ_1} at the transition location, which is more suited to a RANS formulation. The proposed correlation is based on the incompressible flat plate Blasius flow which yields

$$\text{Re}_{\delta_{1tr}} = 1.72 (\text{Re}_{s_{tr}})^{1/2} . \quad (31)$$

They then recast the aforementioned formulations (and proposed a modified form of Walker's model) of $\widetilde{s}_{\text{len}}$ into

$$\text{Re}_{\widetilde{s}_{\text{len}}} = A' (\text{Re}_{\delta_{1tr}})^{b'} . \quad (32)$$

While this version seems well-suited to the RANS approach used in this paper, it suffers from three shortcomings:

- \tilde{s} needs to be evaluated.
- The value of $\widetilde{s}_{\text{len}}$ or $\text{Re}_{\delta_{1tr}}$ is needed downstream of the transition location.
- The correlation that allowed this formulation neglects compressibility and pressure gradient effects

since it is based on a Blasius solution.

The first issue is addressed by noticing that

$$\tilde{s} = \int_{s_{tr}}^s 1 \, d\eta, \quad (33)$$

which is equivalent to integrating a regular N-factor (or solving the corresponding transport equation) with the specific growth rate

$$\sigma_{\tilde{s}} = \begin{cases} 0 & \tilde{I} < 0.2 \\ 1 & \tilde{I} \geq 0.2 \end{cases}. \quad (34)$$

The second one can be dealt with through an additional convection equation (on \widetilde{s}_{len} or $Re_{\delta_{1,tr}}$) with a forcing source term. Finally, the third one would require a new correlation.

The purpose of this type of intermittency model — in the context of this paper — is to get a converged solution more than computing accurately the transitional zone of the flow. For this reason and to simplify the implementation process (*i.e.* to avoid adding a transport equation on \widetilde{s}_{len}), the choice has been made to compute \tilde{s} through the proposed transport equation but to set the intermittency length \widetilde{s}_{len} as a user-defined parameter instead of computing it. For this ONERA-D test case, a transition length $\widetilde{s}_{len}/L = 15\%$ was used in accordance with Stock and Haase's relation (32) and convergence was reached.

Further developments would include the implementation of dedicated intermittency transport equations in a manner closer to the one proposed by Suzen and Huang⁴⁴ which is a combination of the shear flow intermittency model of Cho and Chung⁴⁵ and the longitudinal intermittency model of Steelant and Dick.⁴⁶

V. Application to a laminar transonic airfoil

A 2D transonic laminar airfoil (referred to as Airfoil No. 2) was studied in 2012 by Dassault Aviation and Onera in the context of a European project (the Joint Technology Initiatives, Smart Fixed-Wing Aircraft). The transonic airfoil was tested in Onera's S2MA wind tunnel (Modane-Avrieux Center). Numerical and experimental results are available on this configuration⁴⁷ and the same mesh is used (figure 7(b)) since it has been shown that it is suitable for transition computations. As stated in Hue *et al.*,⁴⁷ it features a classical

C topology known to be suitable to describe the flowfield around this type of airfoil. The total domain length is about 106 chords long, the origin is located at the quarter-chord, and the extent beyond this point is about 57 chords. The whole mesh is made of 215,000 elements, with a stretch ratio of about 1.10 in the boundary layer. Once this grid was computed, Hue *et al.* checked the normalized first cell heights to verify the validity of the boundary-layer discretization and determined that the maximal y^+ on the surface (trailing edge excepted) exhibited values from 0.4 to 1 in the range of Reynolds numbers considered.

The wind tunnel confinement effects are not taken into account in the numerical simulation (free atmosphere configuration), the angle of attack is therefore modified to get the same pressure coefficients in the laminar regions of the airfoil. The experimental lift coefficient is recovered from the integration of the pressure coefficients while the numerical one is obtained *via* the flow circulation around the airfoil. The metrology also features an infrared camera to measure the transition location on the airfoil, pressure taps on the airfoil's skin to get pressure coefficients and a turbulence probe allowing the estimation of the upstream turbulence level.

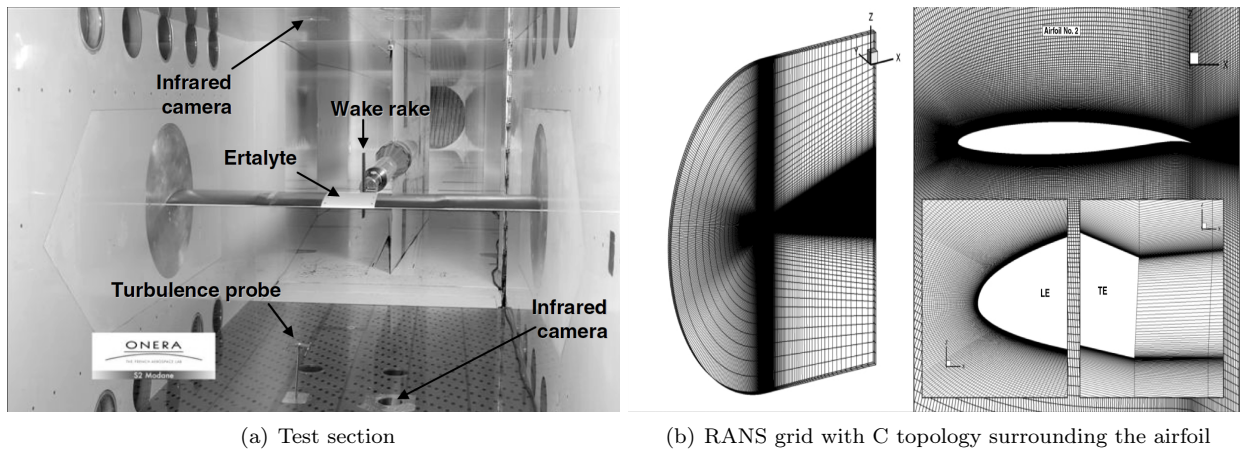


Figure 7. S2MA test section description and *elsA* mesh.

Menter's $k-\omega$ SST model was used but this time the numerical scheme is Roe's second order method with van Albada's limiter. This limiter is necessary since the upstream Mach number in the lot1124 test case (presented table 1) is higher than the airfoil's critical Mach number. A flux-limiter is therefore necessary to capture the resulting discontinuities. It is used on the other cases to ensure the same numerical parameters for all cases.

A three-step approach is used, similar to the one described in section IV:

1. Determine the numerical angle of attack $AoA_{e/sA}$ to get pressure coefficients similar to the experimental ones (iso- K_p conditions) as well as a realistic mean flow and the corresponding boundary-layer quantities. This is done by setting the numerical transition location to the experimental value in e/sA and using a trial and error approach.
2. The boundary-layer quantities obtained during step 1 are input into FENEC to get the range of 20 unstable frequencies whose N-factors will be computed (table 1).
3. The pre-converged flow obtained at step 1 is then used to initialize the complete computation where the 20 N-factor equations are solved to find the numerical transition location $x_{tr,e/sA}$.

A consequence of fulfilling an iso- K_p condition (e/sA_{K_p}) instead of a more classical iso- C_L one (e/sA_{C_L}) is a difference in the numerical and experimental values of C_L . Computations made with values of $AoA_{e/sA}$ ensuring iso- C_L conditions led to discrepancies in pressure distribution resulting in different boundary-layer stability properties. More specifically, the pressure distribution discrepancies were the manifestation of different mean boundary-layer velocity profiles, exhibiting a different set of unstable modes.

Section V.A presents the different test cases configurations as well as an overview of the data-processing methods that were used. Section V.B then presents a detailed analysis of the lot1125 case while section V.C gives an overview of the results obtained on the other lots.

V.A. Overview of test case configurations and data-processing methods

TEST CASE CONFIGURATIONS. Six configurations were used, as summed up in table 1. For each of these cases, transition in the experimental setup was triggered at 5% of chord on the suction side to avoid flow separation. This is also the case for all computations through a forced discontinuous intermittency and all transition prediction results are thus given for the pressure side. The first frequency whose N-factor reaches N_T is responsible for transition and noted f_{tr} .

	M_∞	P_{i_∞} [bar]	T_{i_∞} [K]	Re_L $\times 10^6$	AoA ($^\circ$)		C_L exp.	x_{tr}/L (%) exp.	f [kHz] e/sA
					exp.	e/sA			
lot1126 - Reference	0.70	1.5	300	6.547	0.10	-0.30	0.422	46 - 47	9 - 28
lot1125 - Lower AoA	0.70	1.5	300	6.547	-0.96	-1.40	0.253	32 - 34	26 - 45
lot1124 - Lower AoA	0.70	1.5	300	6.547	-2.00	-2.40	0.096	9 - 10	61 - 80
lot1102 - Higher M_∞	0.73	1.5	300	6.638	0.10	-0.45	0.435	46 - 47	9 - 28
lot1137 - Lower M_∞	0.66	1.5	300	6.373	0.10	-0.43	0.409	46 - 49	9 - 28
lot1078 - Lower Re_L	0.70	1.2	300	5.230	0.10	-0.34	0.427	51 - 53	9 - 28

Table 1. Experimental and numerical flow conditions for the laminar transonic airfoil test cases.

The transition region length is computed using the boundary-layer quantities obtained at the first step (transition location set to the experimental one) and Stock and Haase intermittency length model (yielding $\widetilde{s}_{\text{len}}/L \simeq 10\%$ for each case). No laminar separation occurred for this fixed transition location. Convergence of the final computation (step 3) was considered to be achieved when the conservative variables residuals dropped by 7 to 8 orders of magnitude and the lift and drag coefficients variation between two successive iterations was less than $10^{-5}\%$.

The wind tunnel turbulence level was determined to be of order $T_u \simeq 0.16\%$,⁴⁷ yielding the following value of N_T :

$$N_T = -8.43 - 2.4 \ln(0.16 \times 10^{-2}) \simeq 7.0 . \quad (35)$$

EXPERIMENTAL TRANSITION LOCATION The experimental transition location is given by the change of slope in the temperature evolution (figure 8(b)) extracted from the temperature distribution measured by infrared imaging on the experimental setup (figure 8(a)).

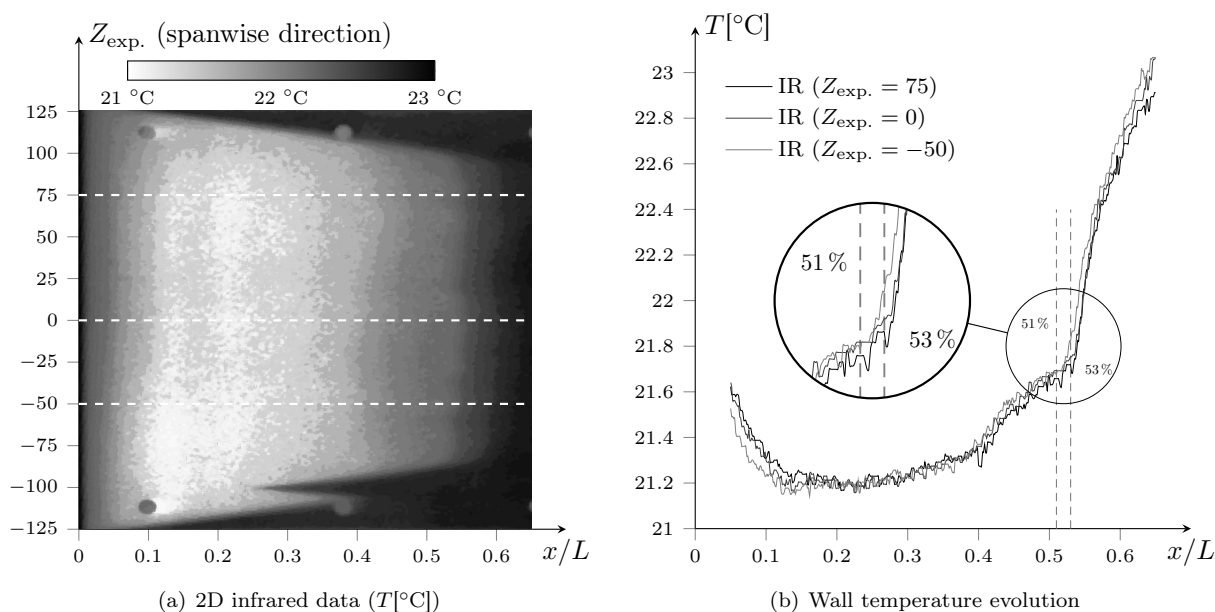


Figure 8. Infrared thermography and transition location (lot1078).

EXACT STABILITY COMPUTATIONS The exact stability computations are performed as follows:

1. inputting some pressure coefficients into 3C3D to get the boundary-layer velocity profiles.
2. using this velocity profiles to get the growth rates *via* the LLS equation.
3. getting the corresponding N-factors through a classical integration.

Two types of exact stability computations are made, depending on which pressure coefficients are chosen:

BL-stab_{iso-K_p} : the pressure coefficients come from the iso- K_p *elsA* results.

BL-stab_{exp.} : the experimental pressure coefficients are used.

V.B. Detailed analysis of lot1125 test case

The lot1125 test case presented the highest error on the transition location when using iso- C_L conditions (table 2). These discrepancies came from an over-estimation of the velocity peak near the leading edge in the *elsA_{C_L}* case leading to a different flow stability and a transition location further upstream than the experimental one.

With the *elsA_{K_p}* configuration, this velocity peak is well recovered (figure 9) and the corresponding transition location given by the Paraboloid method is at 31.9%, in excellent agreement with the expected 32 - 34%.

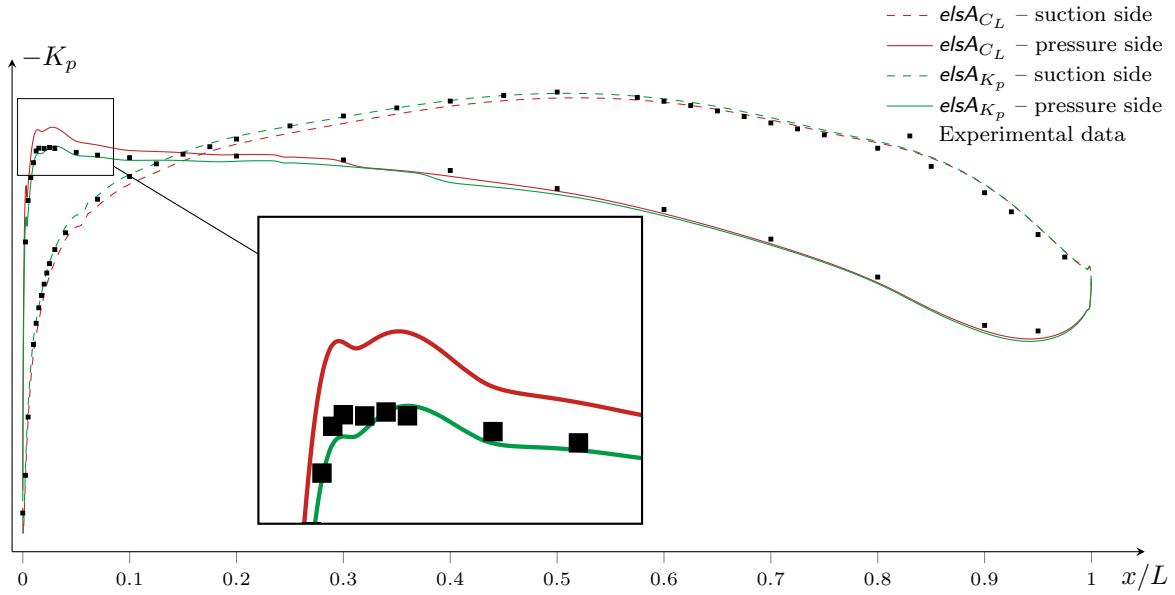


Figure 9. Experimental vs. numerical pressure coefficients distribution (lot1125), iso- C_L ($AoA_{elsA} = -1.61^\circ$).

The Parabolas method in e/sA is compared to the $BL-stab_{iso-K_p}$ and $BL-stab_{exp.}$ exact stability computations. For these three types of computations the values of f_{tr} are respectively 25 kHz, 24 kHz and 23 kHz. The N-factors given by these three frequencies are therefore compared (figure 10).

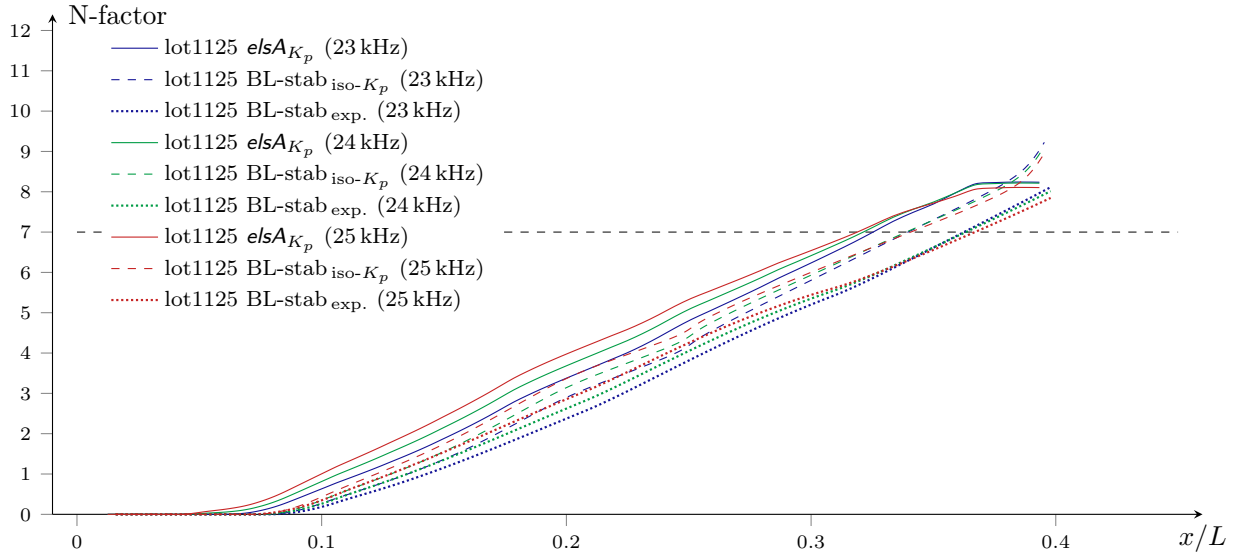


Figure 10. Comparison of N-factors evolution for e/sA_{K_p} , $BL-stab_{iso-K_p}$ and $BL-stab_{exp.}$ (lot1125).

The discrepancies between $BL-stab_{iso-K_p}$ (dashed lines) and $BL-stab_{exp.}$ (dotted lines) show the errors coming from the remaining slight differences in pressure distribution, while the comparison of the N-factors given by e/sA_{K_p} (solid lines) and $BL-stab_{iso-K_p}$ indicate the errors coming from the Parabolas method itself.

They can be broken down into two types:

- An error on the critical abscissa (approx. 3% of chord for $f = 24$ kHz).
- An error on the values of the growth rates.

The error on the values of the growth rates is small enough to have very similar N-factor's slope between the $elsA_{K_p}$ and the BL-stab_{iso- K_p} results. The error on the critical abscissa comes on one hand from the Parabolus method approximation of the critical abscissa and on the other hand from the error made on the boundary-layer quantities input into the Parabolus method in $elsA$. They have respectively been estimated to be of order 1% and 2% of chord for $f = 24$ kHz.

V.C. Overview of results on all cases

V.C.1. Iso- C_L and iso- K_p simulations

Table 2 compares both $elsA_{K_p}$ and $elsA_{C_L}$ results to the experiments for the sake of completeness but only the iso- K_p cases will be considered hereafter.

	AoA ($^\circ$)			C_L		x_{tr}/L (%)		
	exp.	$elsA_{C_L}$	$elsA_{K_p}$	exp.	$elsA_{K_p}$	exp.	$elsA_{C_L}$	$elsA_{K_p}$
lot1126 - Reference	0.10	-0.63	-0.30	0.422	0.471	46 - 47	44.3	46.9
lot1125 - Lower AoA	-0.96	-1.61	-1.40	0.253	0.287	30 - 34	24.1	31.9
lot1124 - Lower AoA	-2.00	-2.52	-2.40	0.096	0.116	9 - 10	6.0	6.9
lot1102 - Higher M_∞	0.10	-0.62	-0.45	0.435	0.459	46 - 47	44.1	47.5
lot1137 - Lower M_∞	0.10	-0.58	-0.43	0.409	0.431	46 - 49	44.5	46.9
lot1078 - Lower Re_L	0.10	-0.53	-0.34	0.427	0.457	51 - 53	47.5	49.3

Table 2. Experimental and numerical results for the laminar transonic airfoil test cases, iso- C_L and iso- K_p .

It is possible in each case to find out which frequency triggers transition, as summed up in table 3. $elsA$'s estimation with the current method presents a satisfactory agreement with the LLS results based on the experimental data.

	lot1126	lot1125	lot1124	lot 1102	lot 1137	lot 1078
f_{tr} ($elsA_{K_p}$)	18 kHz	25 kHz	66 kHz	18 kHz	17 kHz	16 kHz
f_{tr} (BL-stab _{exp.})	17 kHz	23 kHz	77 kHz	18 kHz	16 kHz	16 kHz

Table 3. Comparison of frequencies triggering transition for each case.

The frequency comparison presents limitations as f_{tr} increases since the N-factors begin to weakly depend

on the frequency. Figure 11 shows the evolution of the N-factors at frequencies ranging in a 20 kHz window centered on f_{tr} for the lots 1125 (where the N-factors depend on f) and 1124 (where the N-factors weakly depend on f).

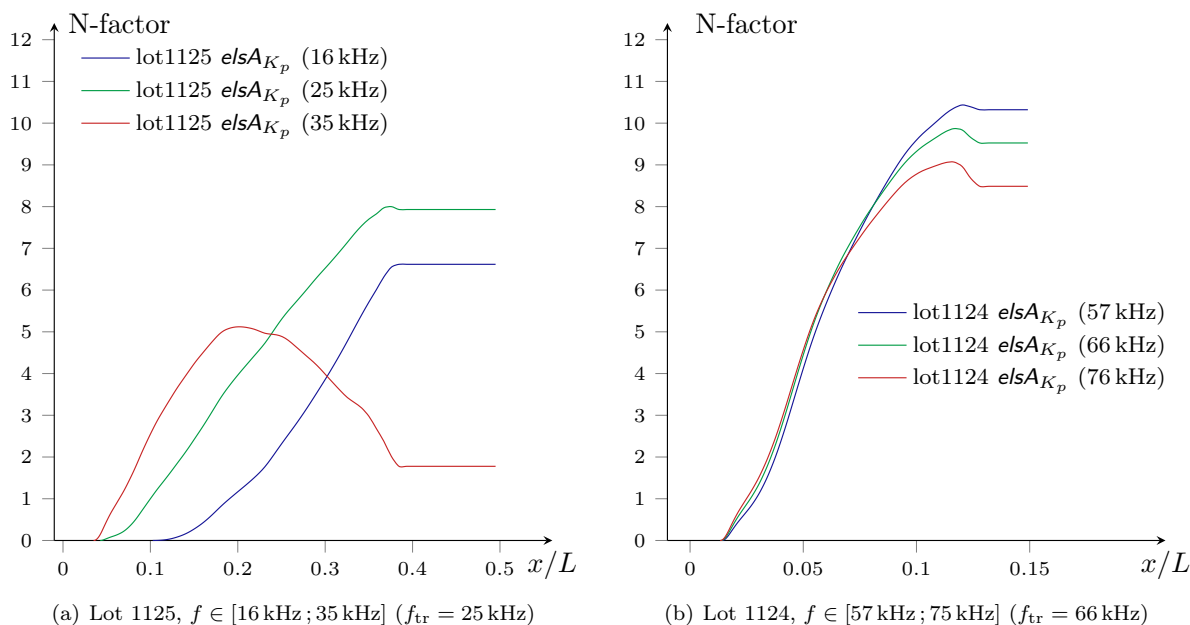


Figure 11. Comparison of the N-factors of lots 1125 and 1124 for a 20 kHz frequency range centered on f_{tr} .

This explains the fact that the highest discrepancies in the prediction of the frequency triggering transition are seen for the lot1124 test case in table 3.

With an iso- K_p criterion for the angle of attack correction, *elsA*'s results are in good agreement with the exact stability computations. This demonstrates that given the right flow configuration the new transition model is able to capture accurately the amplification of the unstable modes.

V.C.2. Mach number, Reynolds number and angle of attack effects on the transition location

This section aims at giving a physical interpretation of the results presented in table 2 for the iso- K_p configurations.

MACH NUMBER EFFECT. Changes in Mach number (lot1102 and lot1137) are not sufficient to observe any noticeable compressibility effects. Transition would be observed further downstream as the Mach number increases because the compressibility effects tend to stabilize perturbations.

REYNOLDS NUMBER EFFECT. A decrease in the Reynolds number Re_L (lot1078) has a stabilizing effect intense enough to observe an expected delayed transition on the experimental setup. The numerical transition location is also observed further downstream.

ANGLE OF ATTACK EFFECT. The decrease in angle of attack amplifies the velocity peak on the pressure side due to the flow bypassing the leading edge. This leads to a decelerated zone, with pressure gradients getting higher as the angle of attack decreases, as can be seen in figure 12. The fast uprising of modes at higher frequencies is therefore fostered and the transition happens further upstream because Tollmien-Schlichting waves are sensitive to adverse pressure gradients.

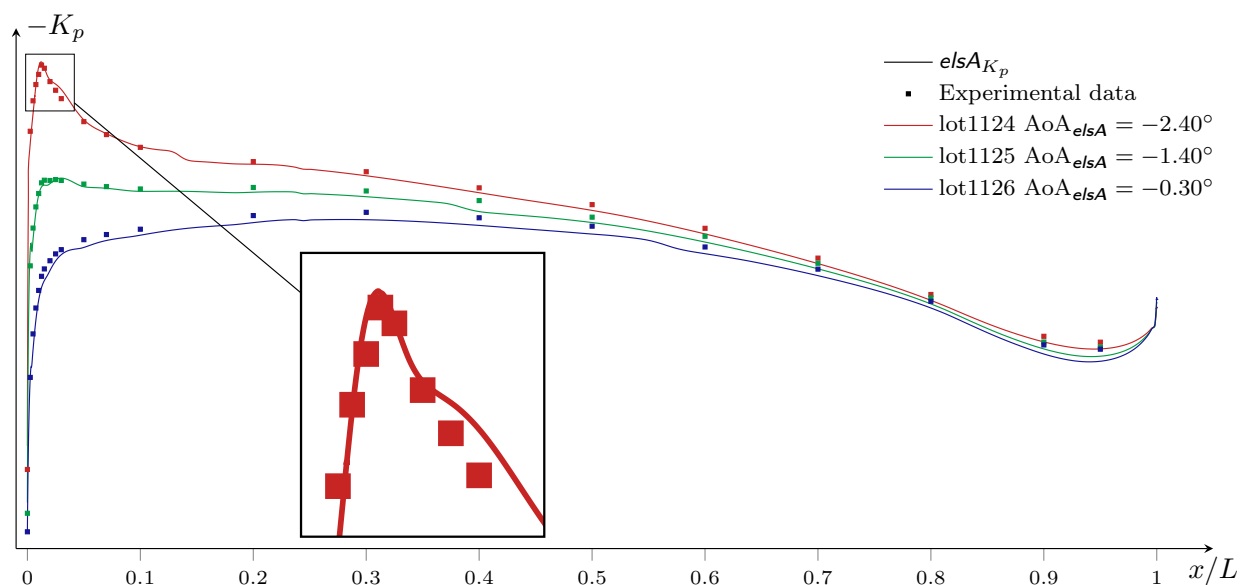


Figure 12. Pressure side experimental vs. numerical pressure coefficients distribution (lots 1124 to 1126), iso- K_p .

VI. Conclusions

A new implementation of the N-factor method in the *elsA* Navier-Stokes solver has been proposed. This new method is based on Onera's database approach and recast the classical N-factor integral formulation into a set of transport equations. The resulting model is better suited for direct RANS applications, however it requires on-the-fly computation of the boundary-layer thickness and integral quantities, which is possible in *elsA*.

It also requires an indicator to check if transition occurred upstream of a given field cell. It has been shown that point transition should not be applied since it is not representative of the real transition process

and generates convergence issues. An exponential law for the intermittency factor has therefore been used.

Computations in the transonic regime were done and successfully validated against experimental results, provided that the numerical angle of attack is chosen to respect the pressure coefficients distribution on the airfoil. This comes directly from the sensitivity of any stability analysis to the boundary-layer flow dynamics, represented by the wall pressure distribution. The iso- C_L condition is very classical when comparing numerical results to experimental ones but this criterion is no longer sufficient when it comes to accurately capturing complex situations such as the laminar-turbulent transition phenomenon.

Further developments will extend the approach to 3D flow cases. The current implementation is already valid for three-dimensional Tollmien-Schlichting waves and crossflow instabilities need to be considered. The computation of the growth rates for this type of instability can be done with the Parabolus method, it requires the determination of some parameters of the generalized inflection point.

An extension of the original database approach also exists to compute transition in separation bubbles. It would therefore be possible to implement this extension and compare its results to the “classical” Gleyzes-Habiballah criterion.

As stated in the abstract, the major benefit of the presented approach is its ability to intrinsically follow the edge streamline without any topology specification from the end user. The additional computational effort is yet to be accurately quantified (in terms of time and memory consumption).

General viscous-inflectional model

This type of instabilities appears at higher Mach numbers or strong adverse pressure gradients. It is the superposition of both viscous and inflectional instabilities. The Parabolus method therefore models their respective growth rates σ_v and σ_i by two sets of two half parabolas. In the end we have

$$\sigma^* = \max(\sigma_v, \sigma_i) , \tag{36}$$

and

$$\frac{\sigma_v}{\sigma_{Mv}} = 1 - \left[\frac{\text{Re}_{\delta_1} - R_{Mv}}{R_{kv} - R_{Mv}} \right]^2 \quad \text{where} \quad R_{kv} = \begin{cases} R_{0v} & \text{Re}_{\delta_1} < R_{Mv} \\ R_{1v} & \text{Re}_{\delta_1} > R_{Mv} \end{cases}, \quad (37a)$$

$$\frac{\sigma_i}{\sigma_{Mi}} = 1 - \left[\frac{\text{Re}_{\delta_1} - R_{Mi}}{R_{ki} - R_{Mi}} \right]^2 \quad \text{where} \quad R_{ki} = \begin{cases} R_{0i} & \text{Re}_{\delta_1} < R_{Mi} \\ R_{1i} & \text{Re}_{\delta_1} > R_{Mi} \end{cases}. \quad (37b)$$

This model loses accuracy when Re_{δ_1} is close to R_{1i} . A linear fix is therefore used as shown in figure 13.

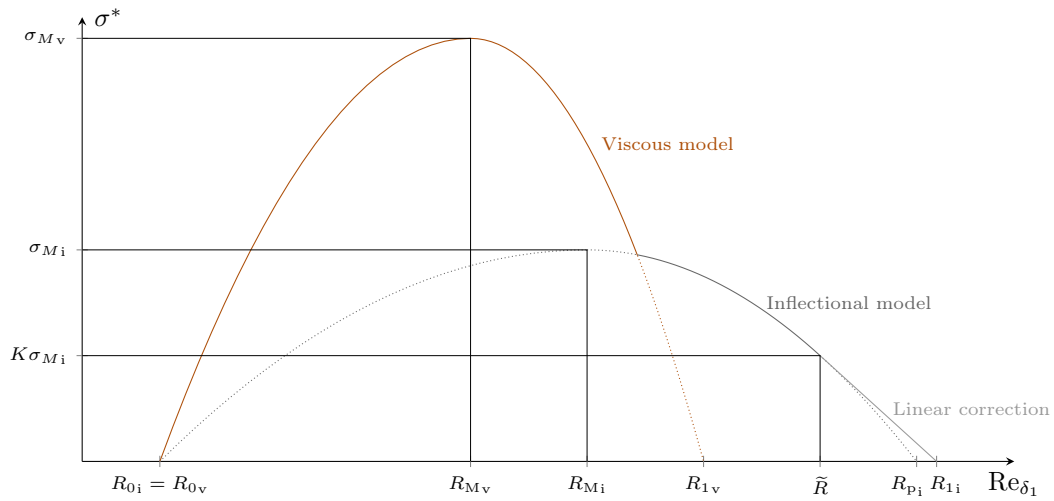


Figure 13. Complete parabolas model with linear correction.

The linear portion is linked to the inflectional model at $\text{Re}_{\delta_1} = \tilde{R}$ and intersects the Re_{δ_1} -axis at R_{1i} .

Growth rates for the respective linear and parabolic parts are thus given by

$$\frac{\sigma_i}{\sigma_{Mi}} = (\text{Re}_{\delta_1} - R_{1i}) \frac{K}{\tilde{R} - R_{1i}}, \quad (38)$$

and

$$\frac{\sigma_i}{\sigma_{Mi}} = 1 - \left[\frac{\text{Re}_{\delta_1} - R_{Mi}}{R_{ki} - R_{Mi}} \right]^2 \quad \text{where} \quad R_{ki} = \begin{cases} R_{0i} & \text{Re}_{\delta_1} < R_{Mi} \\ R_{Pi} & \text{Re}_{\delta_1} > R_{Mi} \end{cases}. \quad (39)$$

Continuity in \tilde{R} and an additional tangent continuity constraint give

$$R_{\text{pi}} = R_{\text{Mi}} - \frac{(R_{\text{Mi}} - \tilde{R})}{\sqrt{1 - K}} \quad \text{and} \quad \tilde{R} = \frac{2(1 - K)R_{1i} + KR_{\text{Mi}}}{2 - K} . \quad (40)$$

$K = 0.5$ was determined to be a good all purpose value and R_{1i} is given by the database. σ_{M_v} is given by

$$\sigma_{M_v} = A_{M_v} \left(1 - \frac{F}{F_{M_v}} \right) . \quad (41)$$

This expression is not valid for a small range of near zero frequencies, where σ_{M_v} does not tend toward a maximum when F decreases but reaches a maximum and then decreases. This behavior occurs at sufficiently large Reynolds numbers to only consider a limiter on σ_{M_v}

$$\sigma_{M_v} = \sigma_{M1} \quad \text{when} \quad F < F_{M_v} \left(1 - \frac{\sigma_{M1}}{A_{M_v}} \right) . \quad (42)$$

The remaining coefficients are functions of F and the whole set of parameters is

$$\sigma_{M_v} = \min \left(A_{M_v} \left(1 - \frac{F}{F_{M_v}} \right), \sigma_{M1} \right) , \quad (43)$$

$$\sigma_{M_i} = A_{M_i} \left(1 - \frac{F}{F_{M_i}} \right) , \quad (44)$$

$$R_{M_v} = K_{M_v} (10^5 F)^{E_{M_v}} , \quad (45)$$

$$R_{M_i} = K_{M_i} (10^5 F)^{E_{M_i}} , \quad (46)$$

$$R_{0_v} = R_{M_v} \left[1 - A_{0_v} \left(1 - \frac{F}{F_{0_v}} \right) \right] , \quad (47)$$

$$R_{0_i} = R_{0_v} , \quad (48)$$

$$R_{1_v} = K_{1_v} (10^5 F)^{E_{1_v}} , \quad (49)$$

$$R_{\text{pi}} = R_{\text{Mi}} - \frac{(R_{\text{Mi}} - \tilde{R})}{\sqrt{1 - K}} , \quad (50)$$

$$R_{1_i} = K_{1_i} (10^5 F)^{E_{1_i}} . \quad (51)$$

The 15 parameters A_{M_v} , F_{M_v} , σ_{M1} , A_{M_i} , F_{M_i} , K_{M_v} , E_{M_v} , K_{M_i} , E_{M_i} , A_{0_v} , F_{0_v} , K_{1_v} , E_{1_v} , K_{1_i} , and E_{1_i} where determined for 32 adiabatic wall configurations and stored in a two entry lookup table based on H_i

and M_e .

Acknowledgements

The authors are grateful to Mr. Hue at Onera (Civil Aircraft Unit) for providing the laminar configuration mesh and his assistance with convergence issues. They also express their appreciation to Mr. Colin at Dassault Aviation for authorizing the publication of results on this same configuration.

References

- ¹van Ingen, J., "The e^N Method for Transition Prediction. Historical Review of Work at TU Delft," *38th Fluid Dynamics Conference and Exhibit*, American Institute of Aeronautics and Astronautics, 2008.
- ²Reed, H. L., Saric, W. S., and Arnal, D., "Linear Stability Theory Applied to Boundary Layers," *Annual Review of Fluid Mechanics*, Vol. 28, No. 1, 1996, pp. 389–428.
- ³van Ingen, J., "A suggested semi-empirical method for the calculation of the boundary layer transition region," Internal report, Delft University of Technology, 1956.
- ⁴Smith, A. M. O. and Gamberoni, N., "Transition, Pressure Gradient and Stability Theory," Tech. Rep. ES 26 388, Douglas Aircraft Company, 1956.
- ⁵Arnal, D., "Transition Prediction in Transonic Flow," *Symposium Transsonicum III*, edited by J. Zierep and H. Oertel, International Union of Theoretical and Applied Mechanics, Springer Berlin Heidelberg, 1989, pp. 253–262.
- ⁶Perraud, J., Arnal, D., Casalis, G., Archambaud, J., and Donelli, R., "Automatic transition predictions using simplified methods," *AIAA Journal*, Vol. 47, 2009, pp. 2676–2684.
- ⁷Squire, H., "On the Stability of Three-Dimensional Disturbances of Viscous Fluid Flow Between Parallel Walls," *Proceedings of the Royal Society A: Mathematical, Physical and Engineering Sciences*, Vol. 142, No. 847, 1933, pp. 621–628.
- ⁸Morkovin, M. V., "On the Many Faces of Transition," *Viscous Drag Reduction*, edited by C. S. Wells, Springer US, 1969, pp. 1–31.
- ⁹Mack, L. M., "Transition Prediction and Linear Stability Theory," *AGARD CP-224*, May 1977.
- ¹⁰Gleyzes, C., Cousteix, J., and Bonnet, J., "Theoretical and experimental study of low Reynolds number transitional separation bubbles," *Conference on Low Reynolds Number Airfoil Aerodynamics*, Notre-Dame, IN, 1985, pp. 137–152.
- ¹¹Abu-Ghannam, B. and Shaw, R., "Natural transition of boundary layer- the effect of turbulence, pressure gradient, and flow history." *Journal of Mechanical Engineering Science*, Vol. 22, No. 5, 1980, pp. 213–228.
- ¹²Arnal, D., Habiballah, M., and Coustols, E., "Laminar instability theory and Transition criteria in two and three-dimensional flow," *La Recherche Aerospatiale (English Edition)*, Vol. 2, 1984, pp. 45–53.
- ¹³Drela, M. and Giles, M. B., "Viscous-Inviscid Analysis of Transonic and Low Reynolds Number Airfoils," *AIAA Journal*,

Vol. 25, No. 10, October 1987, pp. 1347–1355.

¹⁴Drela, M., “MISES Implementation of Modified Abu-Ghannam/Shaw Transition Criterion,” Tech. rep., MIT Aero-Astro, July 1998.

¹⁵Drela, M., “Implicit Implementation of the Full e^N Transition Criterion,” *21st AIAA Applied Aerodynamics Conference*, American Institute of Aeronautics and Astronautics, 2003.

¹⁶Menter, F. R., Langtry, R. B., Likki, S. R., Suzen, Y. B., Huang, P. G., and Völker, S., “A Correlation-Based Transition Model Using Local Variables—Part I: Model Formulation,” *Journal of Turbomachinery*, Vol. 128, No. 3, March 2004, pp. 413–422.

¹⁷Langtry, R. B., Menter, F. R., Likki, S. R., Suzen, Y. B., Huang, P. G., and Völker, S., “A Correlation-Based Transition Model Using Local Variables—Part II: Test Cases and Industrial Applications,” *Journal of Turbomachinery*, Vol. 128, No. 3, March 2004, pp. 423–434.

¹⁸Mayle, R., “The Role of Laminar-Turbulent Transition in Gas Turbine Engines,” *ASME Journal of Turbomachinery*, Vol. 113, 1991, pp. 509–537.

¹⁹Langtry, R. B., “Correlation-Based Transition Modeling for Unstructured Parallelized Computational Fluid Dynamics,” *AIAA Journal*, Vol. 47, No. 12, December 2009, pp. 2894–2906.

²⁰Coder, J. G. and Maughmer, M. D., “Computational Fluid Dynamics Compatible Transition Modeling Using an Amplification Factor Transport Equation,” *AIAA Journal*, Vol. 52, No. 11, November 2014, pp. 2506–2512.

²¹Arnal, D., “Boundary layer transition: predictions based on linear theory,” *In AGARD, Special Course on Progress in Transition Modelling 63 p (SEE N94-33884 10-34)*, Vol. 1, 1994.

²²Cambier, L. and Gazaix, M., “elsA - An efficient object-oriented solution to CFD complexity,” *40th AIAA Aerospace Sciences Meeting & Exhibit*, American Institute of Aeronautics and Astronautics, Jan. 2002.

²³Cliquet, J., Houdeville, R., and Arnal, D., “Application of Laminar-Turbulent Transition Criteria in Navier-Stokes Computations,” *AIAA Journal*, Vol. 46, No. 5, 2008, pp. 1182–1190.

²⁴Stock, H. W. and Degenhart, E., “A simplified e^N method for transition prediction in two-dimensional, incompressible boundary layers,” *Zeitschrift für Flugwissenschaften und Weltraumforschung*, Vol. 13, Feb. 1989, pp. 16–30.

²⁵Fuller, R., Saunders, W., and Vandsburger, U., “Neural network estimation of disturbance growth using a linear stability numerical model,” *35th Aerospace Sciences Meeting and Exhibit*, American Institute of Aeronautics and Astronautics, 1997.

²⁶Crouch, J., Crouch, I., and Ng, L., “Estimating the laminar/turbulent transition location in three-dimensional boundary layers for CFD applications,” *15th AIAA Computational Fluid Dynamics Conference*, American Institute of Aeronautics and Astronautics, 2001.

²⁷Krumbein, A. M., “Automatic Transition Prediction and Application to High-Lift Multi-Element Configurations,” *Journal of Aircraft*, Vol. 42, No. 5, 2005, pp. 1150–1164.

²⁸Raddatz, J. and Fassbender, J. K., “Block Structured Navier-Stokes Solver FLOWer,” *MEGAFLOW-Numerical Flow Simulation for Aircraft Design*, Springer, 2005, pp. 27–44.

- ²⁹Gross, R., Chalot, F., Courty, J.-C., Mallet, M., Tran, D., Arnal, D., and Vermeersch, O., “Automatic transition prediction in an industrial Navier-Stokes solver using higher-order finite elements,” *45th AIAA Fluid Dynamics Conference*, American Institute of Aeronautics and Astronautics, 2015.
- ³⁰Chalot, F., Mallet, M., and Ravachol, M., “A comprehensive finite element Navier-Stokes solver for low and high-speed aircraft design,” *32nd AIAA Aerospace Sciences Meeting, AIAA paper 94-0814*, Reno, 1994.
- ³¹Houdeville, R., “Three-dimensional boundary layer calculation by a characteristic method,” *The 5th Symp. on Num. and Physical Aspects of Aerodynamical Flows*, 1992.
- ³²Prandtl, L., “Bemerkungen über die Entstehung der Turbulenz,” *ZAMM - Journal of Applied Mathematics and Mechanics / Zeitschrift für Angewandte Mathematik und Mechanik*, Vol. 1, No. 6, Jan. 1921, pp. 431–436.
- ³³Hartree, D. R., “On an equation occurring in Falkner and Skan’s approximate treatment of the equations of the boundary layer,” *Mathematical Proceedings of the Cambridge Philosophical Society*, Vol. 33, Cambridge Univ Press, 1937, pp. 223–239.
- ³⁴Lees, L. and Lin, C. C., “Investigation of the Stability of the Laminar Boundary Layer in a Compressible Fluid,” Internal report, California Institute of Technology, Sept. 1946.
- ³⁵Stock, H. W. and Haase, W., “Feasibility Study of eN Transition Prediction in Navier-Stokes Methods for Airfoils,” *AIAA Journal*, Vol. 37, No. 10, 1999, pp. 1187–1196.
- ³⁶Kenwright, D. N., Henze, C., and Levit, C., “Feature extraction of separation and attachment lines,” *IEEE Transactions on Visualization and Computer Graphics*, Vol. 5, No. 2, April 1999, pp. 135–144.
- ³⁷Menter, F., “Zonal Two Equation $k - \omega$ Turbulence Models For Aerodynamic Flows,” *24th Fluid Dynamics Conference*, American Institute of Aeronautics and Astronautics, July 1993.
- ³⁸Roe, P., “Approximate Riemann solvers, parameter vectors, and difference schemes,” *Journal of Computational Physics*, Vol. 43, No. 2, 1981, pp. 357 – 372.
- ³⁹Stock, H. W. and Haase, W., “Navier-Stokes Airfoil Computations with eN Transition Prediction Including Transitional Flow Regions,” *AIAA Journal*, Nov. 2000.
- ⁴⁰Dhawan, S. and Narasimha, R., “Some properties of boundary layer flow during the transition from laminar to turbulent motion,” *Journal of Fluid Mechanics*, Vol. 3, No. 04, Jan. 1958, pp. 418–436.
- ⁴¹Narasimha, R., “A Note on Certain Turbulent Spot and Burst Frequencies,” Tech. Rep. Rept. 78 FM 10, Indian Institute of Science, Bangalore, India, 1978.
- ⁴²Chen, K. K. and Thyson, N. A., “Extension of Emmons’ spot theory to flows on blunt bodies,” *AIAA Journal*, Vol. 9, No. 5, 1971, pp. 821–825.
- ⁴³Walker, G. J., “Transitional flow on axial turbomachine blading,” *AIAA Journal*, Vol. 27, No. 5, 1989, pp. 595–602.
- ⁴⁴Suzen, Y. B. and Huang, P. G., “Modeling of Flow Transition Using an Intermittency Transport Equation,” *Journal of Fluids Engineering*, Vol. 122, No. 2, June 2000, pp. 273–284.
- ⁴⁵Cho, J. R. and Chung, M. K., “A $k - \varepsilon - \gamma$ equation turbulence model,” *Journal of Fluid Mechanics*, Vol. 237, April 1992, pp. 301–322.

⁴⁶Steelant, J. and Dick, E., “Modelling of Bypass Transition with Conditioned Navier–Stokes Equations Coupled to an Intermittency Transport Equation,” *International Journal for Numerical Methods in Fluids*, Vol. 23, No. 3, Aug. 1996, pp. 193–220.

⁴⁷Hue, D., Vermeersch, O., Bailly, D., Brunet, V., and Forte, M., “Experimental and Numerical Methods for Transition and Drag Predictions of Laminar Airfoils,” *AIAA Journal*, Vol. 53, No. 9, 2015, pp. 2694–2712.